ACS OMEGA

Open Access

http://pubs.acs.org/journal/acsodf

Article

Sunlight-Driven Photocatalysis for a Set of 3D Metal−Porphyrin Frameworks Based on a Planar Tetracarboxylic Ligand and Lanthanide Ions

Facundo C. Herrera,[#] Rolando M. Caraballo,[#] Galo J. A. A. Soler Illia, Germán E. Gomez,* and Mariana Hamer*

Cite This: *ACS Omega* 2023, 8, 46777−46785

Read Online

ACCESS | Metrics & More | Article Recommendations | Supporting Information

ABSTRACT: Metal−porphyrin frameworks (MPFs) with trivalent lanthanide ions are the most sought-after materials in the past decade. Their porosities are usually complemented by optical properties imparted by the metal nodes, making them attractive multifunctional materials. Here, we report a novel family of 3D MPFs obtained through solvothermal reactions between tetrakis(4-carboxyphenyl) porphyrin (**H_4TCPP**) and different lanthanide sources, yielding an isostructural family of compounds along the lanthanide series: $[Ln_2(DMF)(\mathbf{TCPP})_{1.5}]$ for Ln = La, Ce, Nd, Pr, Er, Y, Tb, Dy, Sm, Eu, Gd, and Tm. Photoluminescent properties of selected phases were explored at room temperature. Also, the photocatalytic performance exhibited by these compounds under sunlight exposure is promising for its implementation in organic pollutant degradation. In order to study the photocatalytic activity of **Ln-TCPPs** in an aqueous medium, methylene blue (MB) was used as a contaminant model. The efficiency for MB degradation was Sm > Y > Yb > Gd > Er > Eu > either no catalyst or no light, obtaining more than 70% degradation at 120 min with **Sm-TCPP**. These results open the possibility of using these compounds in optical and optoelectronic devices for water remediation and sensing.

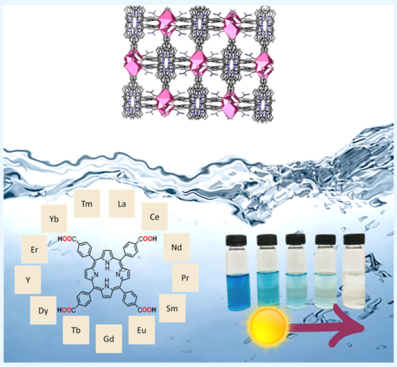

1. INTRODUCTION

Porphyrin molecules and their derivatives play crucial roles in biological systems as light-harvest antennas and catalytic centers. In materials science, these features led to their use as building units to construct multifunctional porous materials that mimic their natural behavior.[1] Therefore, porphyrin-based metal−organic frameworks (MOFs), also called metal−porphyrin frameworks (MPFs), are a kind of porous materials that have raised particular attention due to their distinctive architectures and adaptable chemical functionality, resulting in potential applications in areas such as selective molecular sorption, light-harvesting, heterogeneous catalysis, sensing, and biomedical applications, among other.[1−6]

MPFs have been extensively studied over the past three decades due to the richness of organic linkers and metal node combinations that provide the capacity to tune their light absorption properties.[7] The uniqueness of MPFs also comes from being one of the most intense light absorbers, with the Soret band (400−420 nm) molar absorptivity being as high as 10^5 $L{\cdot}cm^{-1}{\cdot}mol^{-1}$, accompanied by relatively weak lowest-energy Q-band transitions that broaden the light harvest spectra.[8] Furthermore, these optical features could be modified by altering the electronic symmetry postsynthetically.[9] Also, organic linkers with π-conjugated backbones, such as porphyrins, are vastly desirable building blocks for materials with high performance in the photodegradation of dyes because they respond more efficiently to the complete solar spectrum. For example, our group recently reported a set of mesoporous thin films doped with zinc-based exhibiting photocatalytic properties toward dye degradation under sunlight conditions.[10] Moreover, in 2020, we used a Mn−porphyrin to functionalize mesoporous thin films, providing it with the ability to capture volatile organic compounds, resulting in a low-cost sensing device.[11]

On the other hand, trivalent lanthanide ions (Ln^{3+}) are optimal building blocks to construct MOFs with interesting optical properties since they can impart tailored photoluminescent behavior spanning through a broad range, from ultraviolet to visible and near-infrared wavelengths.[12] Besides, depending on the structural features such as the electronic properties from the linker, the involved lanthanide ion, and their relative distance and orientation, ligand-to-metal or metal-to-ligand charge transfer could take place, enhancing "molecular antenna effects" and potential photocatalytic

Received: August 19, 2023
Revised: October 25, 2023
Accepted: November 1, 2023
Published: November 13, 2023

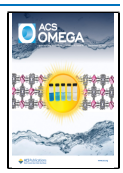

capabilities.[13] The inherent porosity and the large surface area of MOFs pose a significant opportunity for harnessing intermolecular interactions between the framework and a variety of guest molecules. Consequently, variations of their emission spectral profile can be induced by environmental changes and harnessed for sensing[14−16] and photocatalytic purposes.[17] In our previous work, we demonstrated that a correct selection of lanthanide ions and aromatic linkers produced a set of MOFs with visible and near-infrared emissions with thermal-dependent applications.[18]

Due to the oxyphilic nature of lanthanide ions, the most explored porphyrin to construct open frameworks is the tetrakis(4-carboxyphenyl)porphyrin (**H_4TCPP**) ligand.[2,3,19] According to the synthetic conditions, several 2D or 3D structures based on lanthanides and **H_4TCPP** have been reported. As can be seen in Table S1, these crystalline materials have been studied for their applications in luminescence,[20] light-harvesting systems,[21] photocatalysis,[22] photodynamic therapy,[23] anticancer activity,[24] imaging,[25] and as novel structures, with potential applications at the nanoscale.[26,27] For example, Goldberg and co-workers have described the synthesis of open three-dimensional MPFs using **H_4TCPP** combined with lanthanides in an acidic medium,[26,27] while Huang's group has recently reported lanthanide nanosheets based on 2D-MPFs by microwave-assisted synthesis with excellent yields and employed them as photocatalytic platforms toward photo-oxidation of 1,5-dihydroxy naphthalene mediated by *in situ* production of singlet oxygen radicals.[22]

The design of visible-light-active materials is required to maximize the use of solar energy. This goal can be achieved by a rational selection of the antenna-like linkers and different metal ions as nodes.[28] In the present work, we report the synthesis and characterization of a novel isostructural set of 12 MPFs based on **H_4TCPP** along the lanthanide series, belonging to the monoclinic C2/*c* space group, with general formula $[Ln_2(DMF)(\mathbf{TCPP})_{1.5}]$ (with Ln = La, Ce, Nd, Pr, Er, Y, Tb, Dy, Sm, Eu, Gd, and Tm). Their photocatalytic performance was analyzed toward dye degradation in aqueous media under sunlight irradiation. Finally, these results are promising for designing novel photoactive devices with water remediation applications or photodynamic treatment through reactive oxygen species (ROS) generation.

2. EXPERIMENTAL SECTION

2.1. Materials and Reagents. All chemicals were used as received without further purification. Tetrakis(4-carboxyphenyl)porphyrin (**H_4TCPP**) was obtained from Frontier Scientific. Metal sources were purchased from Sigma-Aldrich, Stream Chemicals, or Alfa Aesar, employing $Ln(NO_3)_3{\cdot}xH_2O$ (Ln = Sm, Eu, and Gd), $LnCl_3{\cdot}xH_2O$ (Ln = La, Ce, Nd, Pr, Er, Y, Tb, and Dy), or Ln_2O_3 (Ln = Tm). Ultrapure water was obtained from a Milli-Q system.

2.1.1. Synthesis of ***Ln-TCPP*** *(Ln = La, Ce, Nd, Pr, Sm, Eu, Gd, Tb, Dy, Y, Er, and Tm).* **Ln-TCPP** three-dimensional MPFs were prepared by mixing lanthanide sources and **H_4TCPP** under acidic solvothermal conditions (Scheme S1). The purity of the samples was confirmed by comparison of the experimental and simulated powder X-ray diffraction patterns.

2.2. Characterization. *2.2.1. Powder X-ray Diffraction (PXRD).* Powder X-ray diagrams were obtained on a Rigaku D-MAX-IIIC diffractometer using Cu Kα radiation (λ = 1.5418 Å) with NaCl and quartz as external calibration standards. The best counting statistics were achieved using a scanning step of 0.02° between 5 and 50° Bragg angles, with an exposure time of 5 s per step.

2.2.2. Thermal Analysis. Thermogravimetric analysis (TGA) was performed with a Shimadzu TGA-51 and DSC-60 apparatus under air flowing at 50 mL·min^{-1}. The samples were heated in the 30−800 °C range with a 10 °C·min^{-1} heating rate.

2.2.3. Scanning Electron Microscopy (SEM). images were obtained in a Zeiss LEO1450VP equipment, and energy-dispersive analysis of X-ray spectroscopy (EDS) studies were performed in an EDAX Genesis 2000. Samples were placed on adhesive carbon tape coated with gold.

2.2.4. Nitrogen Gas Sorption Analysis. **Sm-TCPP** was selected for this study. The compound was evacuated in a vacuum oven overnight at room temperature before the gas sorption analysis. ∼50 mg of sample was then transferred to preweighed sample tubes and degassed at 300 °C on a Micromeritics ASAP Gemini model 2380 adsorption analyzer. After degassing, the sample tubes were reweighed to obtain a consistent mass for the samples. Sorption data and BET surface area measurement were collected at 77 K with N_2 using a volumetric technique.[29]

2.2.5. Fourier Transform Infrared Spectroscopy (FTIR). FTIR spectra were recorded with a Nicolet Protégé 460 spectrometer in the 4000−225 cm^{-1} range with 64 scans and a spectral resolution of 4 cm^{-1} by the KBr pellet technique.

2.2.6. UV−vis Spectroscopy. UV−vis spectra of solid **Ln-TCPP** were recorded with a SHIMADZU UV-3600 PLUS UV−vis−NIR spectrometer (185−3300 nm). The photocatalytic measurements were recorded using an Ocean Optics H2 spectrophotometer in a range of 220−1100 nm, resolution 0.08−7.12 nm, illuminating with a deuterium and tungsten lamp, in a 1 cm path length quartz cuvette and using Milli-Q water as blank. All experiments were performed at 25 °C. We also checked that all reactions were unaffected by the irradiation of the sample with the light source of the spectrometer.

2.3. Photocatalysis Experiments. The photocatalytic activity experiments were conducted using an aqueous solution of methylene blue (MB) (10 mg·L^{-1}) containing the **Ln-TCPPs** (100 mg) in Milli-Q water. The suspension was constantly stirred with a magnetic bar for 30 min in dark conditions for 120 min to ensure the establishment of the adsorption/desorption equilibrium, after which the light source was turned on. The suspension was stirred vigorously while being irradiated by a 50 W xenon lamp to simulate sunlight at room temperature. We selected this source because xenon lamps emit a broad spectrum of light that closely resembles natural sunlight in a wide range of wavelengths, including ultraviolet (UV), visible, and infrared (IR) regions.[30−32] The distance between the light source and the cell containing the reaction mixture was set at a constant of 10 cm. The UV−vis absorption spectrum of the sample was monitored at 663 nm (MB absorption maximum) every 2 min for 3 h, using quartz cells. A UV cutoff filter was employed to evaluate the photocatalytic activity under simulated visible sunlight.

3. RESULTS AND DISCUSSION

3.1. Synthesis and Characterizations. Following the synthetic procedure described in Section 2.1.1, 12 **Ln-TCPP** compounds were obtained, washed, and dried at room temperature. The synthesis yield for the dried materials was calculated based on the lanthanide ion as follows: 55% (**La-**

https://doi.org/10.1021/acsomega.3c06153
ACS Omega 2023, 8, 46777−46785

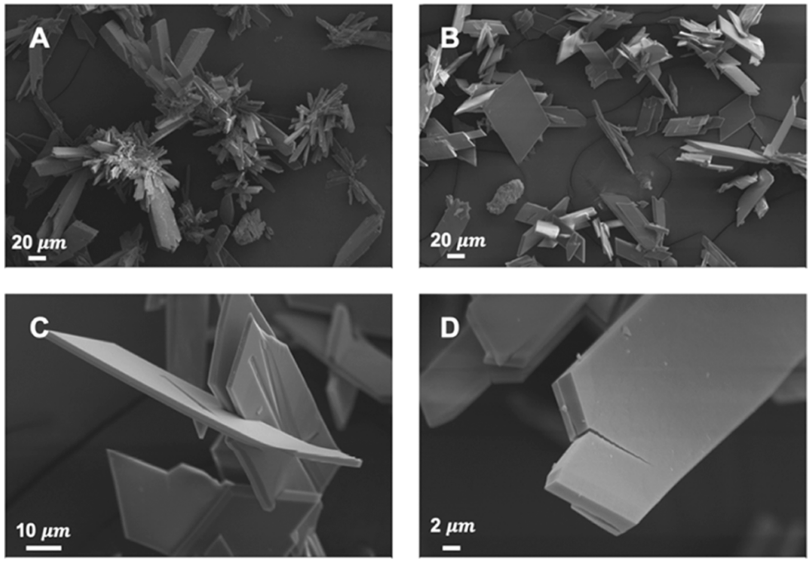

Figure 1. SEM images of **Sm-TCPP** (A), **Er-TCPP** (B), **Y-TCPP** (C), and **Eu-TCPP** (D) compounds.

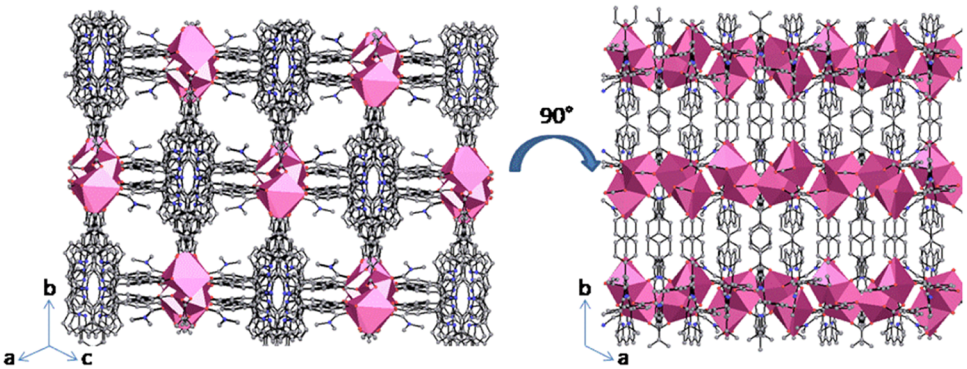

Figure 2. Representation of $[Ln_2(DMF)(\mathbf{TCPP})_{1.5}]$. Hydrogen atoms have been omitted for clarity.

TCPP), 52% (**Ce-TCPP**), 46% (**Nd-TCPP**), 62% (**Pr-TCPP**), 54% (**Er-TCPP**), **45%** (**Y-TCPP**), 38% (**Tb-TCPP**), 45% (**Dy-TCPP**), 12% (**Yb-TCPP**), 72% (**Sm-TCPP**), 44% (**Eu-TCPP**), 53% (**Gd-TCPP**), and 21% (**Tm-TCPP**). The MPFs were then characterized by UV−vis, FTIR spectroscopy, powder X-ray diffraction (XDR), scanning electron microscopy (SEM), thermogravimetric analysis (TGA), and nitrogen gas sorption analysis.

As can be seen in Figure S1, the products consisted of brown crystals with a plate square shape. A more in-depth analysis by the SEM technique made it possible to see the materials in detail, showing crystal aggregations composed of units of around 80 μm in length and 2 μm in thickness (see Figures 1 and S2−S4). EDS analysis (Figure S5) verifies the existence of lanthanide centers.

A unique pure phase along the lanthanide series was confirmed by the PXRD analysis (Figure S6), where their experimental diffraction patterns matched well with those of the simulated one. The compounds are isostructural to the previously reported structure **Nd-(Pt-TCPP)** ($C_{75}H_{46}N_7Nd_2O_{14}Pt_{1.5}$),[27,28,33] crystallizing into the C2/*c* space group. Nevertheless, as far as we know, the synthesized phases described here are new to date, incorporating the majority of lanthanide ions (except for *Pm*, Ho, and Lu), thus exploring not only the phase based on Nd(III). The exclusion of *Pm* is primarily due to its radioactive nature. The omission of Ho and Lu ions stems from their relative rarity compared to most other lanthanides, leading to higher costs. However, they do not exhibit significant chemical differences from the MPFs under investigation.

The secondary building unit (SBU) consists of isolated tetramers of lanthanide ions (Figure S7) connected by three types of $TCPP^{4-}$ linkers in three directions, yielding the three-dimensional structure shown in Figure 2. Two independent crystallographic ions are found, giving rise to irregular hepta- or octacoordinated distorted polyhedra surrounded by oxygen atoms from the linkers and one DMF molecule: $[Nd(1)O_8]$ and $[Nd(2)O_7]$. Based on the organic−inorganic connectivity exhibited by these compounds,[34] the architectures can be classified as I^0O^3, where I^0 means that the inorganic connectivity is 0D and O^3 implies that the organic one is 3D, which involves organic linkers connecting the SBUs in three crystallographic directions; the sum of the exponents results in the overall dimensionality of the structure.

FTIR spectra for **Ln-TCPPs** compounds (Figure S8) showed a predominance of vibrational bands associated with functional groups including carboxylate, methylene, and phenyl moieties. Spectral interpretation was carried out by comparing the observed vibrational bands in **H_4TCPP** with the related compounds.[35] The absence of the C═O stretching at around 1700 cm^{-1} indicates the complete deprotonation of the −COOH groups upon MPF formation. The new bands centered

https://doi.org/10.1021/acsomega.3c06153
ACS Omega 2023, 8, 46777−46785

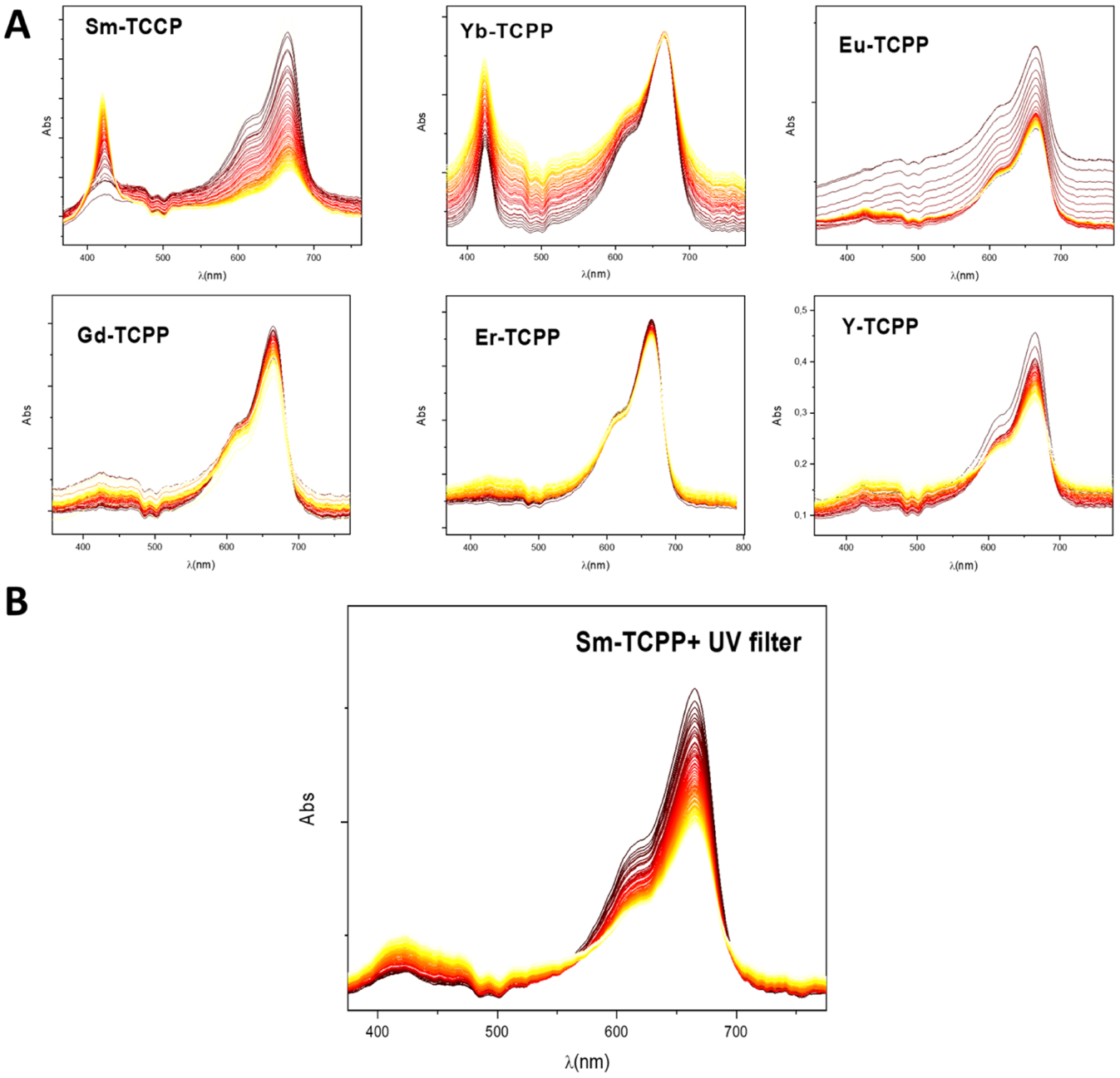

Figure 3. Photocatalytic degradation of an MB water solution (10 mg·L^{-1}) with (A) **Ln-TCPPs** (Ln = Sm, Eu, Gd, Y, Yb, and Er) photocatalysts using UV−vis irradiation and (B) **Sm-TCPP** photocatalyst using UV-filtered visible light irradiation. Experiments were conducted at room temperature for 0−100 min.

at 1606 and 1420 cm^{-1} can be assigned to asymmetric and symmetric vibrational stretchings of COO^-. Also, it is observed that typical porphyrin skeletal modes dominate the spectra in the region of 1000−500 cm^{-1}.

An important insight was provided through thermal analysis regarding the stability of this set of materials. For this study, **Eu-TCPP** and **Er-TCPP** were selected as representative phases. The TGA diagrams show a two-stage evaporation of the solvent (Figure S9). The solvent molecules adsorbed on the crystal surface evaporated below ∼100 °C, while the matrix water and DMF species were lost within the 100−300 °C temperature range. Then, both compounds maintained their mass up to ∼400 °C before decomposing into a black powder upon additional heating.[26] These results are promising for potential applications of these compounds in broad temperature ranges.

The porosity of these **Ln-TCPP** phases was confirmed by the N_2 absorption analysis of **Sm-TCPP**. The N_2 adsorption isotherm shows a type-I(b) profile indicative of the microporous nature of the framework (Figure S10) with a 3.253 Å average adsorption pore width. The BET (Brunauer−Emmett−Teller) specific surface area of the framework was found to have a surface area of 559 m^2/g, while the Langmuir surface was 826 m^2/g. BET analysis indicates a relatively high value since it falls within the scope of values reported for similar TCPP-based MOFs (330−600 m^2/g).[21,36]

The optical properties of the **Ln-TCPP** compounds and the free **H_4TCPP** ligand were explored through UV−vis

https://doi.org/10.1021/acsomega.3c06153
ACS Omega 2023, 8, 46777−46785

absorption spectroscopy. An aqueous solution of **H_4TCPP** exhibits the typical Soret band located at 417 nm and four Q bands centered at 513, 547, 590, and 646 nm (Figure S11). However, the solids did not show any absorption band in water, demonstrating that the porphyrin is part of the crystal lattice and that the MPF structures do not dissolve in water. Furthermore, we confirmed the stability of the MPFs at room temperature and darkness conditions for two years (Figure S12).

3.2. Photophysical and Photocatalytic Experiments. Specific studies have demonstrated that MPFs have been employed as photocatalytic systems for dye degradation and photodynamic therapy involving the generation of reactive oxygen species (ROS).[37−39] As a proof of concept, we analyzed the photocatalytic activity of selected **Ln-TCPPs** (Ln = Sm, Eu, Gd, Y, Er, and Yb) samples with methylene blue (MB) as a model of organic pollutant in an aqueous medium.[40,41] The typical MB absorption band, centered at 663 nm, was monitored to track the reaction progress.[42−46] Figure 3 shows the time-resolved UV−vis absorption spectra of the **Ln-TCPPs** photocatalysts in the 350−750 nm range, registered up to 100 min of irradiation using a xenon lamp source. A continuous decrease in the absorption maximum is observed for **Sm-TCPP** and **Y-TCPP**, denoting the dye degradation. However, the other **Ln-TCPP** compounds showed a moderate band decrease, even smaller than the one obtained with free H_4TCPP.

For **Sm-TCPP**, the appearance of the Soret band at 420 nm (Figure 3A), characteristic of the porphyrin, can be attributed to some degree of superficial breakdown of the **Ln-TCPPs** structure. This would lead to porphyrin release and further degradation upon UV−vis light irradiation. To prevent breakdown and explore the dye degradation under visible light conditions, we performed the same experiment with **Sm-TCPP** using a UV filter during the irradiation process (Figure 3B). The results showed that the dye degradation remains highly efficient while superficial breakdown is minimized.[47]

In order to compare the photocatalytic performance, we analyzed the degradation efficiency of the different **Ln-TCPP** materials, expressed as $(C_0-C)/C_0$, where C_0 is the initial concentration of the MB dye, and C is the concentration at a time t, which can be seen in Figure 4. **Sm-TCPP** showed the highest efficiency, with 55% after 40 min of irradiation and more than 74% after 100 min. The efficiency of MB degradation after 120 min follows the order **Sm-TCPP** > **Y-TCPP** > **Sm-TCPP (UV-filtered)** > **Yb-TCPP** > **Gd-TCPP** > **Er-TCPP** > **Eu-TCPP**. It is worth noting that the degradation of MB in the absence of a photocatalyst was negligible under visible light. However, in the presence of H_4TCPP, the absorption band at 663 nm decreases, and no degradation of the porphyrin ring was observed (Figure S13).

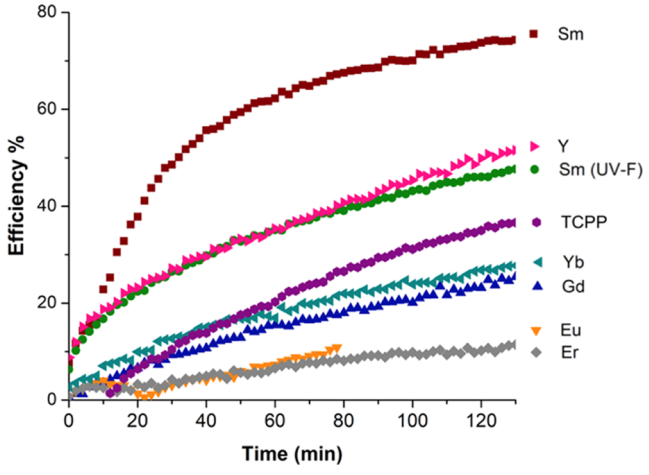

Figure 4. MB photocatalytic degradation efficiency under UV−vis light irradiation for each **Ln-TCPP** and free **H_4TCPP**.

To determine the reaction kinetics of MB degradation catalyzed by the **Ln-TCPP** compounds, a pseudo-first-order model was employed. The data was fitted with a Langmuir−Hinshelwood model equation for analysis (eq 1), where k is the pseudo-first-order rate constant and indicates the photocatalytic activity[48]

$$\ln(C_0/C) = k \cdot t \tag{1}$$

The calculated initial rate constant for each compound is shown in Table 1, together with the comparative photocatalytic efficiency and initial rate constants of selected MOF-based photocatalysts toward MB degradation. The reported values here are comparable to those from MOF structures based on aromatic carboxylic linkers, showing better performance for **Sm-TCPP**.

Based on the significant difference they showed in the MB degradation efficiency and rate constant, we analyzed the solid UV−vis absorption spectra of **Sm-TCPP** and **Eu-TCPP** to elucidate the origin of its differences. From these spectra, the E_g values were estimated through a Tauc plot (Figure 5) (i.e., the curve of converted $(\alpha h\upsilon)^2$ vs $h\upsilon$ from the UV−vis spectrum, where α, υ, A, and E_g are the absorption coefficient, light frequency, proportionality constant, and band gap, respectively). From the plot of $(\alpha h\upsilon)^2$ vs energy (eV), the E_g values were determined by measuring the x-axis intercept of an extrapolated tangential line from the linear regime of the curve. The corresponding E_g values resulted in values of 2.31 and 2.57 eV for **Sm-TCPP** and **Eu-TCPP**, respectively. This could lead to discrepancies observed in their photocatalytic activity since the lower E_g value of a semiconductor, the higher the number of charge carriers that can be energy-promoted, resulting in a better photocatalytic efficiency.[50] The calculated E_g value of **Sm-TCPP** (2.31 eV) is lower, which may explain its exceptional photocatalytic performance compared to that of **Eu-TCPP** and **H_4TCPP**, for which the calculated E_g value was 2.39 eV.

Regarding its photoluminescence properties, this set of MPFs did not evidence the typical lanthanide emission under UV excitation, and their resulting poor photoluminescence was comparable to that from free **H_4TCPP** ligand. Therefore, lanthanide excited states may transfer energy to the ligand excited states from where charge recombination or ROS generation occurs.[50−53] This reasoning is supported for **Sm-TCPP** by the previous determination of E_g. However, it is critical to note that the proposed pathways may vary depending on the presented lanthanide node in the MPF structure, the redox activity of the metal ion, or the location of their excited states, and further studies are needed.

Photodegradation of MB in aqueous solutions in the presence of a photosensitizer could be caused by the initial generation of $^1O_2$, $O_2^{\bullet-}$, or both.[50−53] To determine if these ROS are involved in the degradation of MB, irradiation experiments in the presence of benzoquinone (BQ) were carried out (Figure S14). The MB photodegradation was inhibited substantially in the presence of BQ, resulting in a

https://doi.org/10.1021/acsomega.3c06153
ACS Omega 2023, 8, 46777−46785

Table 1. Comparison of MOFs Based on Aromatic Carboxylic Linkers for Photodegradation of MB

photocatalyst	light source	presence of H_2O_2	MB concentration (mg/L)	time (min)	degradation efficiency (%)	initial rate constants (min^{-1})	refs
Sm-TCPP	Xe lamp	no	10	100	73.8	0.029	this work
	Xe lamp+UV filter	no	10	100	46.0	0.025	this work
Y-TCPP	Xe lamp	no	10	100	49.9	0.022	this work
Yb-TCPP	Xe lamp	no	10	100	26.8	0.007	this work
Er-TCPP	Xe lamp	no	10	100	10.2	0.004	this work
Eu-TCPP	Xe lamp	no	10	100	10.2	0.004	this work
Gd-TCPP	Xe lamp	no	10	100	23.2	0.002	this work
JLNU-101	10 W LED	no	5	90	83.2	0.019	40
$[Cu(4,4'\text{-bipy})Cl]_n$	Xe lamp	yes	10	150	93.9	0.0182	48
$[Co(4,4'\text{-bipy})\cdot(HCOO)_2]_n$	Xe lamp	yes	10	150	54.7	0.0049	48
NC-3	Xe lamp	no	20	100	80.6	0.014	49

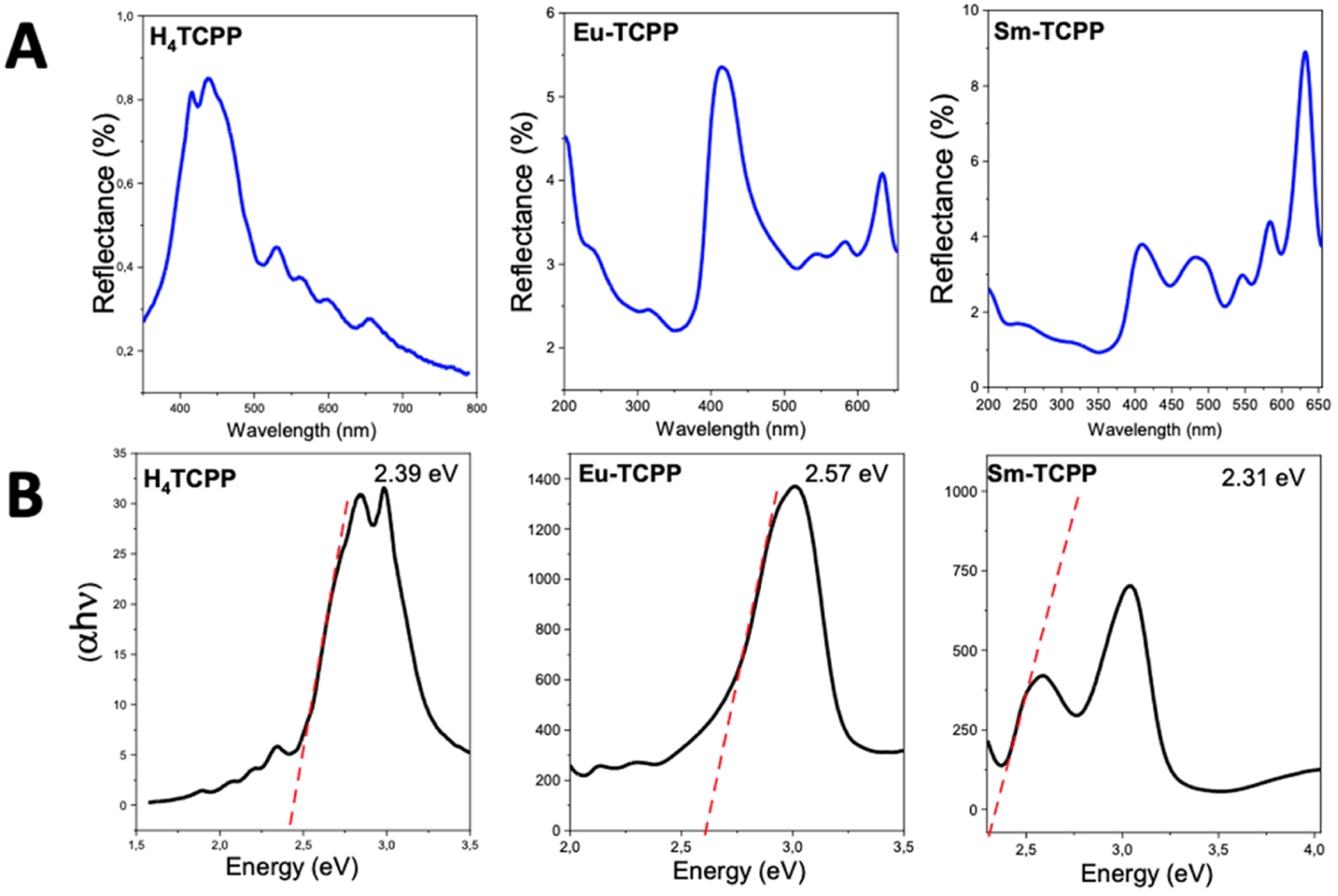

Figure 5. (A) Solid-state UV−vis profiles were identified (blue traces). (B) Band-gap calculation of **Sm-TCPP** and **Eu-TCPP** compounds.

substantial decrease in the degradation efficiency, which could be attributed to BQ quenching the formation of the mentioned through rapid electron transfer to BQ, producing ground-state O_2 and the BQ radical anion.

According to the above experimental data and previous literature findings, a schematic representation of the possible pathways for dye degradation by **Ln-TCPP** is illustrated in Scheme 1. The MB photodegradation process under visible light might be due to different ROS scavengers and mainly attributed to the generation of $O_2^{\bullet-}$ anion.[50−53] These ROS have the potential to initiate the oxidation of MB in aqueous media, resulting in the formation of smaller molecules or inorganic species.[40] The generation of these ROS species could have different origins, but the MPFs we present seem to be formed via the energy transfer from the ^{3}TCPP ligand excited state. At the same time, the population of ^{3}TCPP could be enhanced through the interaction with lanthanide nodes,

https://doi.org/10.1021/acsomega.3c06153
ACS Omega 2023, 8, 46777−46785

Scheme 1. Proposed Sensitized Dye Photodegradation by Employing Ln-TCPP Phases under Sunlight Irradiation (TCPP: Porphyrin Ligand; MB: Methylene Blue; Ln: Trivalent Lanthanide Ion; ISC: Intersystem Crossing)

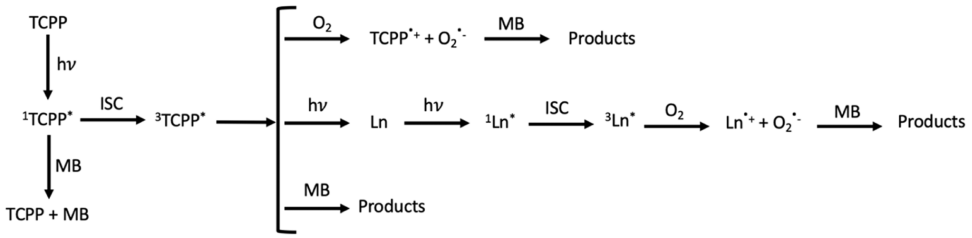

where further research is needed to elucidate its mechanisms completely.

In summary, MB was rapidly decomposed under both ultraviolet and visible irradiations by **Sm-TCPP** through ROS generation. Considering the data above, the node nature might play a relevant role in the MB degradation.

4. CONCLUSIONS

A set of 12 metal−porphyrin frameworks (MPFs) based on a planar tetrakis(4-carboxyphenyl) porphyrin ligand and lanthanide ions were successfully obtained using a one-step solvothermal method. All of the obtained compounds, with the formula $[Ln_2(DMF)(\mathbf{TCPP})_{1.5}]$ (Ln^{3+} = La, Ce, Nd, Pr, Er, Y, Tb, Dy, Sm, Eu, Gd, and Tm), belong to a 3D isostructural family that crystallizes into the monoclinic C2/*c* space group. The overall characterization was carried out by employing a set of techniques in the solid state: PXRD, FTIR, ATG, UV−vis spectroscopy, and scanning electron microscopy. Due to the exceptional light absorption properties of the building blocks, the compounds were evaluated as potential sunlight-driven photocatalysts toward MB degradation in aqueous media. Six members were selected, and their photocatalytic efficiency was analyzed. Due to its narrow band gap, **Sm-TCPP** exhibited the highest catalytic performance with a degradation of 74% of MB within 100 min. Furthermore, it is postulated that the photodegradation is mediated by superoxide and hydroxyl radicals produced under sunlight irradiation of **Ln-TCPP** due to their porous nature. Finally, it is important to remark on the multifunctional profile of the reported materials for light-harvesting, heterogeneous catalysis, photodynamic therapy, thin-film devices, optics, and optoelectronic applications, making a substantial contribution to the lanthanide−organic framework community.

■ ASSOCIATED CONTENT

Supporting Information

The Supporting Information is available free of charge at https://pubs.acs.org/doi/10.1021/acsomega.3c06153

Ln-TCPP reported structure; **Ln-TCPP** synthetic procedure; optical micrographs of **Ln-TCPP**; SEM micrographs and EDS profiles of **Sm-TCPP, Eu-TCPP, Er-TCPP, and Y-TCPP**; experimental **Ln-TCPP** compounds PXRD patterns compared to the simulated Nd-(Pt-TCPP) pattern; scheme of the tetramers units in **Ln-TCPP** compounds; FTIR spectra of all of the **Ln-TCPP** compounds and $\mathbf{H_4TCPP}$ ligand; TGA profiles of **Er-TCPP** and **Eu-TCPP** compounds; nitrogen adsorption isotherm of **Sm-TCPP**; UV−vis spectrum of $\mathbf{H_4TCPP}$ ligand in water; and photocatalytic degradation of MB water solution in the presence of $\mathbf{H_4TCPP}$ using UV−vis light irradiation (PDF)

■ AUTHOR INFORMATION

Corresponding Authors

Germán E. Gomez − *Instituto de Investigaciones en Tecnología Química (INTEQUI-CONICET), Universidad Nacional de San Luis, Área de Química General e Inorgánica, Facultad de Química, Bioquímica y Farmacia (UNSL-FQByF), 1455 San Luis, Argentina*; Email: gegomez@unsl.edu.ar

Mariana Hamer − *Instituto de Ciencias, Universidad Nacional de General Sarmiento-CONICET, CP1613 Los Polvorines, Argentina*; orcid.org/0000-0002-2391-2913; Email: mhamer@campus.ungs.edu.ar

Authors

Facundo C. Herrera − *Instituto de Nanosistemas, Escuela de Bio y Nanotecnología, Universidad Nacional de General San Martín (INS-UNSAM)-CONICET, 1650 San Martín, Argentina; Laboratorio Argentino Haces de Neutrones-Comisión Nacional de Energía Atómica, 1499 Villa Maipú, Argentina*

Rolando M. Caraballo − *Instituto de Ecología y Desarrollo Sustentable (INEDES), Universidad Nacional de Luján (UNLu-CONICET), 6700 Luján, Argentina*; orcid.org/0000-0003-0471-2446

Galo J. A. A. Soler Illia − *Instituto de Nanosistemas, Escuela de Bio y Nanotecnología, Universidad Nacional de General San Martín (INS-UNSAM)-CONICET, 1650 San Martín, Argentina*

Complete contact information is available at: https://pubs.acs.org/10.1021/acsomega.3c06153

Author Contributions

#F.C.H. and R.M.C. participated equally in the development of this work. F.C.H. and R.M.C.: investigation, visualization, and writing—original draft. G.J.A.A.S.I.: funding acquisition, resources, discussions, and writing—review. G.E.G.: investigation, visualization, formal analysis, resources, supervision, and writing—original draft (lead). M.H.: conceptualization, investigation, visualization, formal analysis, funding acquisition, resources, supervision, and writing—original draft (lead).

Notes

The authors declare no competing financial interest.

■ ACKNOWLEDGMENTS

This work was supported by the CONICET (PIP 11220210100917CO), UNSAM, Agencia I+D+i PICT 2017-4651, PICT 2018-04236, PICT 2020-03130. PICT-2018-

https://doi.org/10.1021/acsomega.3c06153
ACS Omega 2023, 8, 46777−46785

03583 (UNSL), and PICTO 2021-UNGS 00002. F.C.H. thanks the Agency for its grant and the National Atomic Energy Commission for its support. M.H., R.M.C., G.E.G., and G.J.A.A.S.I. are members of CONICET.

REFERENCES

(1) De, S.; Devic, T.; Fateeva, A. Porphyrin and Phthalocyanine-Based Metal Organic Frameworks beyond Metal-Carboxylates. *Dalton Trans.* **2021**, *50* (4), 1166−1188.
(2) Guo, Z.; Chen, B. Recent Developments in Metal−Metalloporphyrin Frameworks. *Dalton Trans.* **2015**, *44* (33), 14574−14583.
(3) Zhang, X.; Wasson, M. C.; Shayan, M.; Berdichevsky, E. K.; Ricardo-Noordberg, J.; Singh, Z.; Papazyan, E. K.; Castro, A. J.; Marino, P.; Ajoyan, Z.; et al. A Historical Perspective on Porphyrin-Based Metal−Organic Frameworks and Their Applications. *Coord. Chem. Rev.* **2021**, *429*, No. 213615.
(4) Chen, L.-J.; Zhao, X.; Yan, X.-P. Porphyrinic Metal-Organic Frameworks for Biological Applications. *Adv. Sens. Energy Mater.* **2023**, *2* (1), No. 100045.
(5) Rajasree, S. S.; Li, X.; Deria, P. Physical Properties of Porphyrin-Based Crystalline Metal−organic Frameworks. *Commun. Chem.* **2021**, *4* (1), No. 47.
(6) Chen, J.; Zhu, Y.; Kaskel, S. Porphyrin-Based Metal−Organic Frameworks for Biomedical Applications. *Angew. Chem., Int. Ed.* **2021**, *60* (10), 5010−5035.
(7) Wang, C.-C.; Zhang, Y.-Q.; Zhu, T.; Wang, P.; Gao, S.-J. Photocatalytic Degradation of Methylene Blue and Methyl Orange in a Zn(II)-Based Metal−Organic Framework. *Desalin. Water Treat.* **2016**, *57* (38), 17844−17851.
(8) Haldar, R.; Batra, K.; Marschner, S. M.; Kuc, A. B.; Zahn, S.; Fischer, R. A.; Bräse, S.; Heine, T.; Wöll, C. Bridging the Green Gap: Metal−Organic Framework Heteromultilayers Assembled from Porphyrinic Linkers Identified by Using Computational Screening. *Chem. - Eur. J.* **2019**, *25* (33), 7847−7851.
(9) Marschner, S. M.; Haldar, R.; Fuhr, O.; Wöll, C.; Bräse, S. Modular Synthesis of Trans -A 2 B 2 -Porphyrins with Terminal Esters: Systematically Extending the Scope of Linear Linkers for Porphyrin-Based MOFs. *Chem. - Eur. J.* **2021**, *27* (4), 1390−1401.
(10) Caraballo, R. M.; Vensaus, P.; Herrera, F. C.; Soler Illia, G. J. A. A.; Hamer, M. Zinc Porphyrin/Mesoporous Titania Thin Film Electrodes: A Hybrid Material Nanoarchitecture for Photocatalytic Reduction. *RSC Adv.* **2021**, *11* (49), 31124−31130.
(11) Caraballo, R. M.; Onna, D.; López Abdala, N.; Soler Illia, G. J. A. A.; Hamer, M. Metalloporphyrins into Mesoporous Photonic Crystals: Towards Molecularly-Tuned Photonic Sensing Devices. *Sens. Actuators, B* **2020**, *309*, No. 127712.
(12) Armelao, L.; Quici, S.; Barigelletti, F.; Accorsi, G.; Bottaro, G.; Cavazzini, M.; Tondello, E. Design of Luminescent Lanthanide Complexes: From Molecules to Highly Efficient Photo-Emitting Materials. *Coord. Chem. Rev.* **2010**, *254* (5−6), 487−505.
(13) Gomez, G. E.; Roncaroli, F. Photofunctional Metal-Organic Framework Thin Films for Sensing, Catalysis and Device Fabrication. *Inorg. Chim. Acta* **2020**, *513*, No. 119926.
(14) Lustig, W. P.; Mukherjee, S.; Rudd, N. D.; Desai, A. V.; Li, J.; Ghosh, S. K. Metal−Organic Frameworks: Functional Luminescent and Photonic Materials for Sensing Applications. *Chem. Soc. Rev.* **2017**, *46* (11), 3242−3285.
(15) Gomez, G. E.; dos Santos Afonso, M.; Baldoni, H. A.; Roncaroli, F.; Soler-Illia, G. J. A. A. Luminescent Lanthanide Metal Organic Frameworks as Chemosensing Platforms towards Agrochemicals and Cations. *Sensors* **2019**, *19* (5), 1260.
(16) Ortega, F. G.; Gomez, G. E.; Boni, C.; García, I. C.; Navas, C. G.; D'vries, R. F.; D'vries, R. F.; Molina Vallejos, M. P.; Serrano, M. J.; Messina, G. A.; Hernández, J. E. Microfluidic Amperometric Immunosensor Based on Porous Nanomaterial towards Claudin7 Determination for Colorectal Cancer Diagnosis. *Talanta* **2023**, *251*, No. 123766.
(17) Wang, J.-L.; Wang, C.; Lin, W. Metal−Organic Frameworks for Light Harvesting and Photocatalysis. *ACS Catal.* **2012**, *2* (12), 2630−2640.
(18) Gomez, G. E.; Marin, R.; Carneiro Neto, A. N.; Botas, A. M. P.; Ovens, J.; Kitos, A. A.; Bernini, M. C.; Carlos, L. D.; Soler-Illia, G. J. A. A.; Murugesu, M. Tunable Energy-Transfer Process in Heterometallic MOF Materials Based on 2,6-Naphthalenedicarboxylate: Solid-State Lighting and Near-Infrared Luminescence Thermometry. *Chem. Mater.* **2020**, *32* (17), 7458−7468.
(19) Huh, S.; Kim, S.-J.; Kim, Y. Porphyrinic Metal−Organic Frameworks from Custom-Designed Porphyrins. *CrystEngComm* **2016**, *18* (3), 345−368.
(20) Chen, X. Conditional Controlled Nano Coordination Polymers with Tunable Full Color Light Emitting. *Dyes Pigm.* **2021**, *188*, No. 109169.
(21) Yang, S.; Hu, W.; Nyakuchena, J.; Fiankor, C.; Liu, C.; Kinigstein, E. D.; Zhang, J.; Zhang, X.; Huang, J. Unravelling a Long-Lived Ligand-to-Metal Cluster Charge Transfer State in Ce−TCPP Metal Organic Frameworks. *Chem. Commun.* **2020**, *56* (90), 13971−13974.
(22) Jiang, Z. W.; Zou, Y. C.; Zhao, T. T.; Zhen, S. J.; Li, Y. F.; Huang, C. Z. Controllable Synthesis of Porphyrin-Based 2D Lanthanide Metal−Organic Frameworks with Thickness- and Metal-Node-Dependent Photocatalytic Performance. *Angew. Chem., Int. Ed.* **2020**, *59* (8), 3300−3306.
(23) Gao, Z.; Chen, F.; Li, Y.; Zhang, Y.; Cheng, K.; An, P.; Sun, B. A Small-Sized and Stable 2D Metal−Organic Framework: A Functional Nanoplatform for Effective Photodynamic Therapy. *Dalton Trans.* **2019**, *48* (45), 16861−16868.
(24) Liu, J.-C.; Gu, J.-J.; Zhang, Y.-S. Synthesis, Crystal Structure, and Anti-Breast Cancer Activity of a Novel Metal-Porphyrinic Complex [YK(TCPP)(OH)2·(Solvents)X]. *Braz. J. Med. Biol. Res.* **2018**, *51* (1), No. e6858, DOI: 10.1590/1414-431x20176858.
(25) Zhao, Y.; Kuang, Y.; Liu, M.; Wang, J.; Pei, R. Synthesis of Metal−Organic Framework Nanosheets with High Relaxation Rate and Singlet Oxygen Yield. *Chem. Mater.* **2018**, *30* (21), 7511−7520.
(26) Lipstman, S.; Muniappan, S.; George, S.; Goldberg, I. Framework Coordination Polymers of Tetra(4-Carboxyphenyl)-Porphyrin and Lanthanide Ions in Crystalline Solids. *Dalton Trans.* **2007**, No. 30, 3273.
(27) Muniappan, S.; Lipstman, S.; George, S.; Goldberg, I. Porphyrin Framework Solids. Synthesis and Structure of Hybrid Coordination Polymers of Tetra(Carboxyphenyl)Porphyrins and Lanthanide-Bridging Ions. *Inorg. Chem.* **2007**, *46* (14), 5544−5554.
(28) Singh, A.; Singh, A. K.; Liu, J.; Kumar, A. Syntheses, Design Strategies, and Photocatalytic Charge Dynamics of Metal−Organic Frameworks (MOFs): A Catalyzed Photo-Degradation Approach towards Organic Dyes. *Catal. Sci. Technol.* **2021**, *11* (12), 3946−3989.
(29) Thommes, M.; Kaneko, K.; Neimark, A. V.; Olivier, J. P.; Rodriguez-Reinoso, F.; Rouquerol, J.; Sing, K. S. W. Physisorption of Gases, with Special Reference to the Evaluation of Surface Area and Pore Size Distribution (IUPAC Technical Report). *Pure Appl. Chem.* **2015**, *87* (9−10), 1051−1069.
(30) Parupudi, R. V.; Singh, H.; Kolokotroni, M. Sun Simulator for Indoor Performance Assessment of Solar Photovoltaic Cells. *Energy Procedia* **2019**, *161*, 376−384.
(31) Dibowski, G.; Esser, K. Hazards Caused by UV Rays of Xenon Light Based High Performance Solar Simulators. *Saf. Health Work* **2017**, *8* (3), 237−245.
(32) Esen, V.; Sağlam, Ş.; Oral, B. Light Sources of Solar Simulators for Photovoltaic Devices: A Review. *Renewable Sustainable Energy Rev.* **2017**, *77*, 1240−1250.
(33) Jiang, Z. W.; Zou, Y. C.; Zhao, T. T.; Zhen, S. J.; Li, Y. F.; Huang, C. Z. Controllable Synthesis of Porphyrin-Based 2D Lanthanide Metal−Organic Frameworks with Thickness- and Metal-Node-Dependent Photocatalytic Performance. *Angew. Chem.* **2020**, *132* (8), 3326−3332.

https://doi.org/10.1021/acsomega.3c06153
ACS Omega 2023, 8, 46777−46785

(34) Cheetham, A. K.; Rao, C. N. R.; Feller, R. K. Structural Diversity and Chemical Trends in Hybrid Inorganic−Organic Framework Materials. *Chem. Commun.* **2006**, No. 46, 4780−4795.
(35) Nakamoto, K. *Infrared and Raman Spectra of Inorganic and Coordination Compounds*, 5th ed.; John Wiley & Sons, Inc.: USA, 1997.
(36) Rhauderwiek, T.; Heidenreich, N.; Reinsch, H.; Øien-Ødegaard, S.; Lomachenko, K. A.; Rütt, U.; Soldatov, A. V.; Lillerud, K. P.; Stock, N. Co-Ligand Dependent Formation and Phase Transformation of Four Porphyrin-Based Cerium Metal−Organic Frameworks. *Cryst. Growth Des.* **2017**, *17* (6), 3462−3474.
(37) He, T.; Ni, B.; Zhang, S.; Gong, Y.; Wang, H.; Gu, L.; Zhuang, J.; Hu, W.; Wang, X. Ultrathin 2D Zirconium Metal-Organic Framework Nanosheets: Preparation and Application in Photocatalysis. *Small* **2018**, *14* (16), No. 1703929.
(38) Ma, Y.; Li, X.; Li, A.; Yang, P.; Zhang, C.; Tang, B. H 2 S-Activable MOF Nanoparticle Photosensitizer for Effective Photodynamic Therapy against Cancer with Controllable Singlet-Oxygen Release. *Angew. Chem., Int. Ed.* **2017**, *56* (44), 13752−13756.
(39) Liu, Y.; Moon, S.-Y.; Hupp, J. T.; Farha, O. K. Dual-Function Metal−Organic Framework as a Versatile Catalyst for Detoxifying Chemical Warfare Agent Simulants. *ACS Nano* **2015**, *9* (12), 12358−12364.
(40) Jiang, W.; Li, J.; Jiang, Y.; Zhou, S.; Liu, B.; Zhou, T.; Liu, C.; Che, G. A 3D Porphyrinic Metal-Organic Framework with Fsc Topology for Efficient Visible-Light-Driven Photocatalytic Degradation. *Polyhedron* **2022**, *226*, No. 116091.
(41) Dar, U. A.; Beig, S. U. R. Remediation of Methylene Blue Dye in Aqueous Solution Using Structurally Diverse and Porous In(III)Chloride Metalloporphyrins. *J. Mol. Struct.* **2023**, *1273*, No. 134372.
(42) Houas, A. Photocatalytic Degradation Pathway of Methylene Blue in Water. *Appl. Catal., B* **2001**, *31* (2), 145−157.
(43) Sakatani, Y.; Grosso, D.; Nicole, L.; Boissière, C.; de A A Soler-Illia, G. J.; Sanchez, C. Optimised Photocatalytic Activity of Grid-like Mesoporous TiO 2 Films: Effect of Crystallinity, Pore Size Distribution, and Pore Accessibility. *J. Mater. Chem.* **2006**, *16* (1), 77−82.
(44) Drisko, G. L.; Zelcer, A.; Wang, X.; Caruso, R. A.; Soler-Illia, G. J. de A. A. Synthesis and Photocatalytic Activity of Titania Monoliths Prepared with Controlled Macro- and Mesopore Structure. *ACS Appl. Mater. Interfaces* **2012**, *4* (8), 4123−4130.
(45) Lu, Q.; Zhang, Y.; Liu, S. Graphene Quantum Dots Enhanced Photocatalytic Activity of Zinc Porphyrin toward the Degradation of Methylene Blue under Visible-Light Irradiation. *J. Mater. Chem. A* **2015**, *3* (16), 8552−8558.
(46) Jiang, Z. W.; Zhao, T. T.; Li, C. M.; Li, Y. F.; Huang, C. Z. 2D MOF-Based Photoelectrochemical Aptasensor for SARS-CoV-2 Spike Glycoprotein Detection. *ACS Appl. Mater. Interfaces* **2021**, *13* (42), 49754−49761.
(47) Rasheed, T. Water Stable MOFs as Emerging Class of Porous Materials for Potential Environmental Applications. *Chemosphere* **2023**, *313*, No. 137607.
(48) Zhang, M.; Wang, L.; Zeng, T.; Shang, Q.; Zhou, H.; Pan, Z.; Cheng, Q. Two Pure MOF-Photocatalysts Readily Prepared for the Degradation of Methylene Blue Dye under Visible Light. *Dalton Trans.* **2018**, *47* (12), 4251−4258.
(49) Shan, C.; Zhang, X.; Ma, S.; Xia, X.; Shi, Y.; Yang, J. Preparation and Application of Bimetallic Mixed Ligand MOF Photocatalytic Materials. *Colloids Surf., A* **2022**, *636*, No. 128108.
(50) Yu, X.; Li, W.; Li, Z.; Liu, J.; Hu, P. Defect Engineered Ta2O5 Nanorod: One-Pot Synthesis, Visible-Light Driven Hydrogen Generation and Mechanism. *Appl. Catal., B* **2017**, *217*, 48−56.
(51) Dejneka, M. J.; Streltsov, A.; Pal, S.; Frutos, A. G.; Powell, C. L.; Yost, K.; Yuen, P. K.; Müller, U.; Lahiri, J. Rare Earth-Doped Glass Microbarcodes. *Proc. Natl. Acad. Sci. U.S.A.* **2003**, *100* (2), 389−393.
(52) Gao, Y.; Suh, M.-J.; Kim, J.-H.; Yu, G. Imparting Multifunctionality in Zr-MOFs Using the One-Pot Mixed-Linker Strategy: The Effect of Linker Environment and Enhanced Pollutant Removal. *ACS Appl. Mater. Interfaces* **2022**, *14* (21), 24351−24362.
(53) Schlachter, A.; Asselin, P.; Harvey, P. D. Porphyrin-Containing MOFs and COFs as Heterogeneous Photosensitizers for Singlet Oxygen-Based Antimicrobial Nanodevices. *ACS Appl. Mater. Interfaces* **2021**, *13* (23), 26651−26672.

https://doi.org/10.1021/acsomega.3c06153
ACS Omega 2023, 8, 46777−46785